Analytical and Bioanalytical Chemistry
https://doi.org/10.1007/s00216-020-02605-9

RESEARCH PAPER

Dynamic light scattering biosensing based on analyte-induced inhibition of nanoparticle aggregation

A. D. Levin[1] · A. Ringaci[2] · M. K. Alenichev[1] · E. B. Drozhzhennikova[1] · K. G. Shevchenko[2,3] · V. R. Cherkasov[2,3] · M. P. Nikitin[2] · P. I. Nikitin[3]

Received: 18 November 2019 / Revised: 20 February 2020 / Accepted: 17 March 2020

Abstract

A new approach to direct quantitative detection of small molecules (haptens) by dynamic light scattering biosensing is presented. The proposed technique implements a homogeneous competitive immunoassay and is based on optical detection of specific inhibition of nanoparticle aggregation induced by the analyte in a sample. The technique performance was tested both in buffer and milk for detection of chloramphenicol – antibiotic relevant to food safety diagnostics. Good specificity, sensitivity (LOD in milk is 2.4 ng/ml), precision (4.0 ± 1.2%), ruggedness (8.3%), and 96% recovery in conjunction with a record wide dynamic range (3 orders of magnitude) of the nanosensing technique were demonstrated. Such characteristics complemented by the assay simplicity (no washing step) and a short assay time make the approach attractive for application as an analytical platform for point-of-care and field-oriented diagnostics.

Keywords Optical biosensor · Homogeneous assay · Chloramphenicol · Gold nanoparticles · Magnetic nanoparticles

Introduction

Direct optical detection methods have been steadily gaining more attention in recent years due to the possibilities they provide for development of fast and easy-to-handle analytical assays, the results of which are not compromised by probe labeling [1]. This tendency is heavily supported by recent regulatory guidelines that require testing of new medical devices in situ conditions rather in vitro. Immobilization of a bioreagent and detection of its binding with a soluble counterpart is one of the most popular concepts for direct biosensing. Usually, the solid phase is represented by flat gold films or Schottky structures for surface plasmon resonance (SPR) sensors [2, 3], and surface of a waveguide or a glass chip for interferometry sensors [4]. The signal may be detected as a change in thickness of the adsorbed layer, in the refraction index values, etc. However, all these methods require elaborate preparation of sample or surface modification. In this connection, direct biosensing that employs the phenomenon of elastic light scattering including the dynamic light scattering (DLS) and a distributed surface of nanoparticles, rather than a flat one of a biochip, represents an appealing alternative, especially in the light of recent advances in nanotechnologies [5–9]. The combination of ligand carrier properties with sophisticated tracer functionality has determined a wide spread of nanoparticles, whose field of use extends from analytical and diagnostic applications [10] to the engineering of advanced "smart" nanoconstructions for biomedicine and theranostics [11–14].

Published in the topical collection *Advances in Direct Optical Detection* with guest editors Antje J. Baeumner, Günter Gauglitz, and Jiri Homola.

A. D. Levin and A. Ringaci contributed equally to this work.

Electronic supplementary material The online version of this article (https://doi.org/10.1007/s00216-020-02605-9) contains supplementary material, which is available to authorized users.

✉ A. D. Levin
levin-ad@vniiofi.ru

✉ M. P. Nikitin
max.nikitin@phystech.edu

P. I. Nikitin
nikitin@kapella.gpi.ru

[1] All-Russian Research Institute for Optical and Physical Measurements, 46 Ozernaya st., 119361 Moscow, Russia

[2] Moscow Institute of Physics and Technology, 9 Institutskii per., 141700 Dolgoprudny, Moscow Region, Russia

[3] Prokhorov General Physics Institute of the Russian Academy of Sciences, 38 Vavilov St, 119991 Moscow, Russia

Published online: 12 April 2020

Such sensing platforms are based on direct optical registration of the temporal dependence of laser intensity scattered by hybrid nano-objects, such as functionalized nanoparticles, in the course of their biospecific aggregation. The obtained data are subjected to further mathematical processing and are presented as a dependence of size of the aggregated nano-objects from the analyte concentration [15]. This approach was successfully applied to quantitative detection and analysis of a wide range of chemical and biological targets [16]. For instance, the DLS-based nanosensors were developed for registration of proteins and nucleic acids [17, 18], tumor markers [19–22], viruses and viral pathogens [23–25], several transgene products [26], and toxic metal ions [27]. The application of DLS-based nanosensors for direct detection and analysis in no-wash point-of-care diagnostics is of special interest and importance [3, 28].

Currently, there are two major immunoassay concepts for analyte detection – sandwich [29] and competitive [30] assays. In the case of DLS optical biosensing, most assays are sandwich-type and involve nanoparticle conjugates with two different antibodies as an immunological pair. When these two types of nanoparticles are mixed in a sample solution that contains antigen (analyte), a specific binding causes the nanoparticles to form aggregates. The resulting shift in average particle hydrodynamic diameter (AHD) can be detected by DLS and directly correlates to the analyte concentration [6]. A similar concept may be applied for detection of the target molecules with several identical epitopes. In this case, only one type of nanoparticle-antibody conjugates may be used. Generally, the sandwich-type DLS assays are characterized by good sensitivity but their use is limited to detection of large multi-epitope analytes in a very narrow range of concentrations.

Here, we propose an alternative approach for DLS-based detection of small single-epitope analytes in a competitive-type assay. To the best of our knowledge, this is the first DLS-based nanosensor that employs a simple but effective concept of a decrease in the size of nanoparticle aggregates upon increase of analyte concentration due to competitive binding between the analyte molecules in a solution and the ones immobilized on the surface of the nanoparticles. Chloramphenicol (CAP) was chosen as a representative model analyte to validate the proposed concept.

CAP is an antibiotic, which is effective against a wide range of bacterial infections in both humans and animals. However, when administered on a regular basis even in small concentrations, it may cause serious side effects, such as Gray syndrome and fatal aplastic anemia. This fact has led to the complete ban of CAP by the FDA in the USA, as well as by the EC authorities [31]. However, in the most of low- and middle-income countries, it is still in the toolbox for animal use due to its low price. Thus, development of a reliable, sensitive, rapid, and robust assay for CAP is of vital importance for these countries.

Existing analytical methods for CAP detection include label-free interferometric biosensors [30], enzyme-linked immunosorbent assay (ELISA) [31], high-performance liquid chromatography (HPLC) [32], gas chromatography–mass spectrometry (GC–MS) [33], and quartz crystal microbalance (QCM) [34]. All these methods have excellent characteristics in terms of accuracy and sensitivity. However, their wide application is limited due to the high cost and complicated sample processing that requires qualified personnel. In this case, the use of nanoparticles (NPs) as multimodal probes is promising. In the last years, optical NP-based sensors for CAP detection were developed that exploit quantum dots fluorescence [35], surface-enhanced Raman scattering (SERS) [36], and localized surface plasmon resonance (LSPR) in functionalized gold nanoparticles [37, 38].

Operational concept of the nanosensor

The proposed approach employs nanoparticles as a quasi-homogenous solid phase for immobilization of an analyte and its receptor, which are usually represented by an antigen-antibody pair. First, a suspension of antibody-functionalized nanoparticles (conjugate A) is mixed with the sample and incubated for several minutes. The analyte molecules bind to antibodies on the nanoparticle surface, decreasing the number of "vacant" antibodies. Then, the nanoparticles functionalized by the analyte are added (conjugate B), and the mixture is incubated for 30 min. If all analyte molecules in the solution are bound, the average fraction of vacant antibodies on the conjugate A surface can be expressed as:

$$\eta_{\mathrm{vac}} = \eta_0 - \frac{10^{-3} \cdot C \cdot N_{\mathrm{Av}}}{\eta_{\mathrm{c\_A}}} \tag{1}$$

where $\eta_{\mathrm{c\_A}}$ is the number concentration of the conjugate nanoparticles A (cm^{-3}); η_0 is the total number of antibodies per nanoparticle; C is the molar concentration of the analyte; and N_{Av} is the Avogadro constant. The derivation of this formula and simulation of the target molecule capturing on conjugate A surface using Langmuir kinetic equation [39] are outlined in Section S1 of the Electronic Supplementary Material (ESM).

At the second stage, conjugates A and B aggregate at a rate that depends on their concentrations, the constants of analyte-receptor association and dissociation rates, and the concentration of "vacant" antibodies on the nanoparticle surface after exposure. The aggregation model that takes into account the blockade of antibody fraction on the surface of conjugate A is also given in Section S1 of ESM. The model is based on the Smolukhovsky coagulation theory [40] and substantiates the proposed approach theoretically.

For the special case of dimer formation at the initial stage of aggregation, the time dependence of AHD of the single- and double-particle aggregate mixture can be expressed as follows [41]:

$$\frac{d_h(t)}{d_h(0)} = 1 + \frac{I_2}{2 \cdot I_1}\left(1 - \frac{d_{h1}}{d_{h2}}\right) k_{11} N_0 t + \ldots \quad (2)$$

where I_1 and I_2 are the light scattering intensities of single conjugates and dimers, respectively; d_{h1} and d_{h2} are their hydrodynamic diameters; k_{11} is the aggregation rate constant; t is the reaction time; and N_0 is the total concentration of single conjugate types A and B at the initial time. For the biospecific aggregation of conjugates during incubation, this constant is proportional to the fraction of vacant antibodies on conjugate A surface (see details in Section S1.2 of ESM). Thus, as it follows from Eqs. (1) and (2), the smaller the average size of the conjugates at the end of incubation, the greater the analyte concentration in the sample. The average conjugate size after incubation is measured using DLS.

The proposed system implements a competitive no-wash immunoassay in the DLS format (Fig. 1). Indeed, the analyte molecules compete with conjugate B for binding to the antibodies on the surface of conjugate A. The target molecules have a privileged position due to much smaller size and, therefore, higher diffusion coefficient compared with that of conjugate B.

Next, we have experimentally demonstrated the feasibility of such nanosensor using detection of CAP as a model. The feasibility was shown in both end point and kinetic modes.

Materials and methods

Materials

The following reagents and materials were used: chloramphenicol (CAP), bovine serum albumin (BSA), trisodium citrate dihydrate, phosphate buffer saline (PBS) (all from Sigma-Aldrich, Germany); monoclonal mouse anti-chloramphenicol CAPB10 antibodies (Mabs, Russian Research Center for Molecular Diagnostics and Therapy, Russia); chloroauric acid (Dragtsvetmet, Russia). Gentamicin (Dalchimpharm, Russia) and lincomycin (Belmedpreparaty, Belarus) antibiotics were used. Sterilized milk for baby food of 3.2% fat mass fraction was purchased from a local grocery store. All other auxiliary reagents were of analytical grade and were used without further purification.

Carboxylated polystyrene-coated magnetic 0.2 μm beads Estapor with high (MH1-020/50, SPION-H) and lower (M1-020/50, SPION-L) concentration of surface carboxyl groups and Red Fluorescent PS Latex Beads 0.31 μm were purchased from Merck Millipore (France) and Magsphere Inc (USA), respectively. The gold nanoparticles (40 ± 5 nm) were prepared by citrate reduction of $HAuCl_4$ solution according to the modified Turkevich protocol [42].

Methods

The conjugates of magnetic nanoparticles with CAP-BSA conjugate or anti-CAP antibody were prepared via adapted carbodiimide method [43]. Briefly, 200 μg of nanoparticles was mixed with the solution of 9 mg EDC and 4.5 mg S-NHS in 20 μl of 50 mM MES buffer (pH 5). The resulting mixture was sonicated for 20 min at RT, and 25 μg of protein in borate buffer (pH 8) was added. After overnight incubation, the nanoparticles were washed thrice and resuspended in 80 μl of 1% BSA in PBS (pH 7.4).

Latex Beads conjugates were obtained via passive adsorption according to the manufacturer recommendations in PBS (pH 7.4). The resulting nanoparticles were washed out by repeated centrifugation and finally resuspended in 80 μl of 1% BSA in PBS.

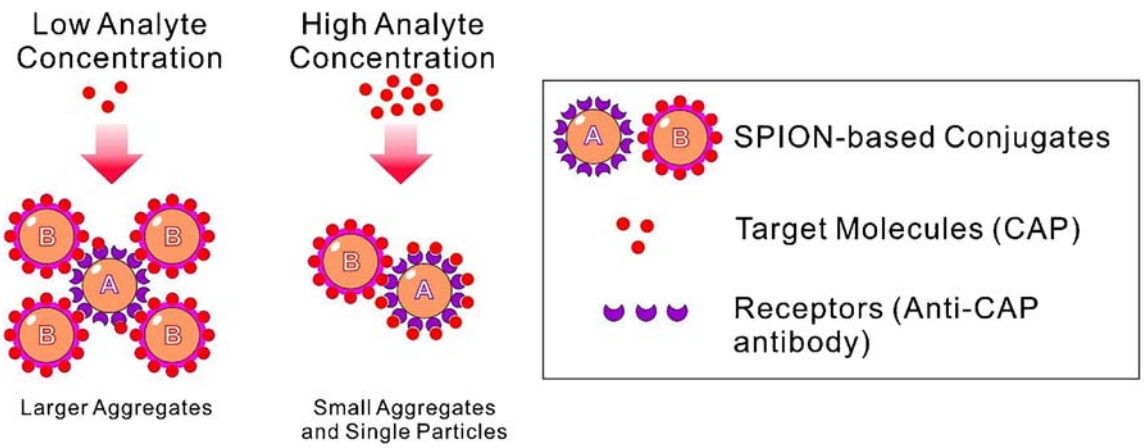

Fig. 1 Schematic representation of the proposed assay principle: on the left – conjugates aggregation at low analyte concentration, most antibodies are vacant after the first stage, large aggregates are formed at the second stage; on the right – high analyte concentration, most antibodies were occupied at the first stage and small aggregates are formed at the second stage

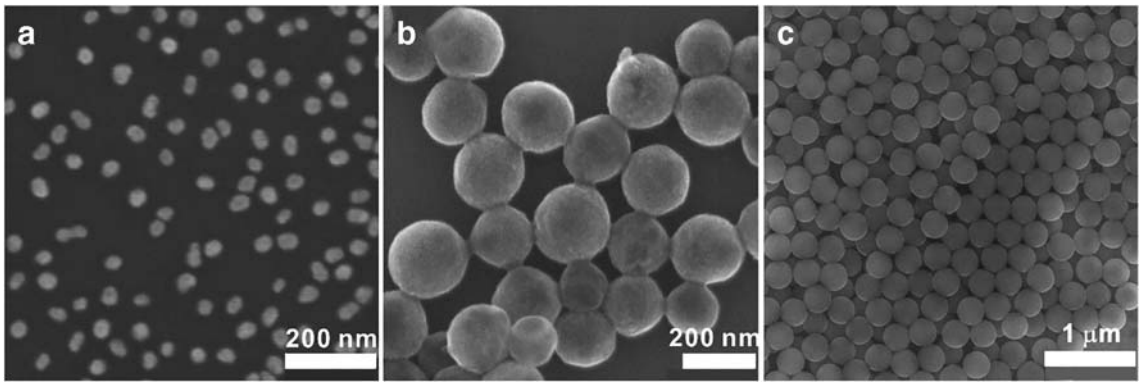

Fig. 2 Scanning electron microscopy (SEM) images of gold (**a**), SPION (**b**), and Red Fluorescent PS Latex (**c**) nanoparticles

Conjugation of gold nanoparticles was carried out as described previously [44]. Briefly, 0.8 ml of gold nanoparticle suspension (OD = 0.66 at 530 nm) was added to 100 μg of CAP-BSA or 45 μg of antibodies (conjugation with antibodies was carried out at pH 9 adjusted with 0.05 M NaOH). After 2–3-min incubation, 0.2 ml of 5% BSA in PBS (pH 7.4) was added; the mixture was washed three times with 1% BSA in PBS by centrifugation and resuspended in 100 μl of 1% BSA in PBS. CAP-BSA auxiliary conjugate was obtained by incubation of chloramphenicol succinate (CAP-suc) with EDC and S-NHS dissolved in 50% DMSO and 50% 50 mM MES buffer (pH 5) for 2 h. Next, BSA in borate buffer (pH 8) was added with molar ratio BSA:CAP-Suc:EDC:NHS = 1:40:80:80. The mixture was incubated overnight and washed with Zeba desalting column.

Scanning electron microscopy (SEM) images were obtained with a MAIA3 (Tescan, Czech Republic) microscope at accelerating voltage of 10 kV. The samples were diluted down to appropriate concentrations, placed onto silicon wafer, and then allowed to dry at the ambient conditions.

DLS assay in buffer solution. Various sample preparation algorithms were tested, differing in concentrations of the conjugates and the ratios between the conjugates and the analyte.

According to the basic protocols for end point measurements, 10 μl of 1% BSA solution in PBS was mixed with CAP sample solutions of various concentrations (from 0 to 10^6 ng/ml). Then, the conjugate A solution (10 μl of latex (2.5 g/l), gold NPs (50 pM), or 5 μl Estapor magnetic beads (2.5 g/l)) was added, and the mixture was incubated for 5 min. After that, the conjugate B solution (10 μl of latex (2.5 g/l), gold NPs (50 pM), or 5 μl of Estapor beads (2.5 g/l)) was added and incubated for 30 min at 37 °C. Finally, the solution was diluted to 2 ml with PBS, and AHD was measured by DLS.

DLS assay in milk. The CAP stock solution (1 g/l) was prepared by mixing 2.7 ml of the milk with 0.3 ml of CAP ethanol solution (10 g/l). The milk samples with different CAP concentrations were prepared by the stock dilution with unspiked milk in the certain proportions.

Then, 10 μl of the obtained solution was mixed with 10 μl of 1% BSA-PBS solution followed by adding of 5 μl of

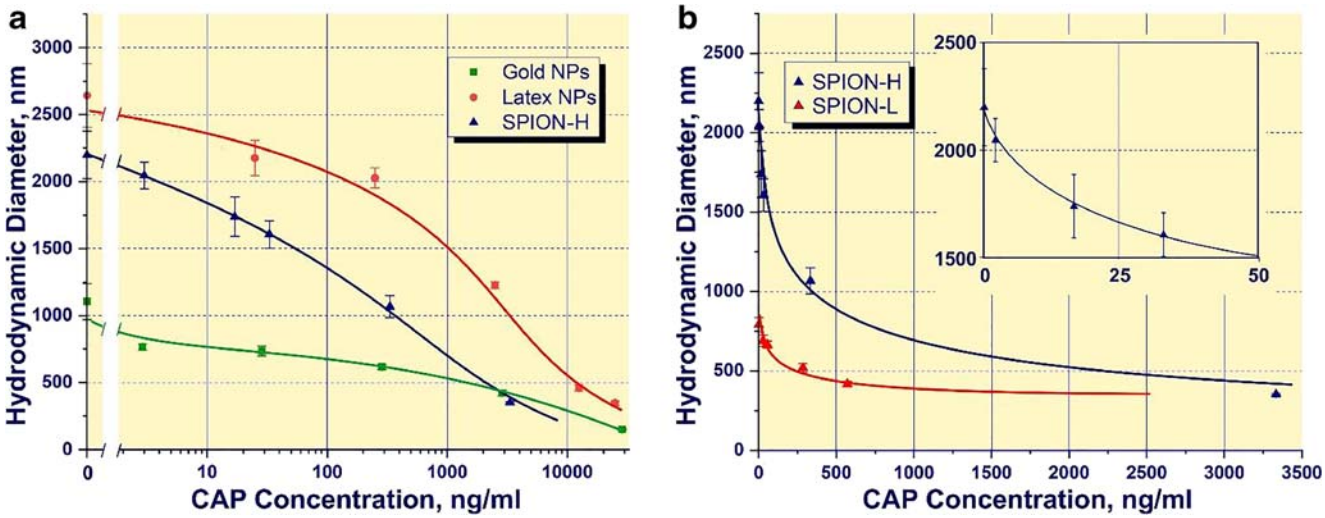

Fig. 3 Dependences of the nanoparticle AHD vs. CAP concentration in the working buffer: **(a)** semi-log scale for three types of conjugates based on gold, SPION-H, and latex NPs; **(b)** linear scale for SPION-H and SPION-L (higher- and lower-carboxylated)-based conjugates (the insert shows larger scale fragment for SPION-H). Error bars correspond to standard deviation

SPION-L-based conjugate A solution, vortexing, and 5-min incubation. Conjugate A was then precipitated using a permanent magnet. The collected pellet was resuspended in 20 μl of 1% BSA-PBS and sonicated, and 5 μl of pre-sonicated SPION-L-based conjugate B was added. The resulting mixtures were incubated at 37 °C for 30 min, then dissolved in 1 ml of PBS in a DLS cuvette, and AHD was measured by an ARN-2 analyzer.

A recovery test was carried out by mixing of three CAP solutions of known concentrations (53.3, 266.7, and 533.3 ng/ml in the working buffer) in equal proportions (1:1) followed by comparison of the calculated and the measured values of the increase in concentrations. Five independent measurements were performed. The overall assay recovery (R) was calculated as a mean of the ratios between the measured (Cm) and actual increments of CAP concentration (Ca) in the samples: $R\ (\%) = (\mathrm{Cm}/\mathrm{Ca}) \times 100$.

In the kinetic studies, the incubation was carried out directly in the DLS analyzer thermostated cuvette (total volume 300 μl, including 10 μl analyte, 5 μl solutions of conjugates of types A and B, 280 μl PBS) at 10 times lower concentration of reagents than at the end point measurements.

Instrumentation

The nanoparticle size analyzer ARN-2 developed by "VNIIOFI" (Russia) and described in [45] was used for end point measurements. The assay was performed at the scattering angle 90° in a 3.5-ml Kartell polystyrene cuvette with path length of 10 mm. For the kinetic studies, a Malvern Zetasizer Nano ZS analyzer with the scattering angle 172° and 70–850-μl Brand UV microcuvettes was used.

Results and discussion

End point measurements

To demonstrate the flexibility of the proposed approach and its independence on the nature of analyzing nanoparticles, we have tested the bioconjugates of anti-CAP Mabs with gold, latex, and superparamagnetic (SPION) nanoparticles (see Fig. 2 and ESM Fig. S1 for SEM images and DLS characteristics of the initial NPs, respectively).

All tested NPs showed satisfactory performance in the CAP assay (Fig. 3a), while the most reproducible data and best limit of detection (LOD) were obtained for conjugates based on gold NPs and SPION (4.0 and 11.5 ng/ml, respectively). The magnetic particles permit easy manipulation and measuring DLS in opaque mediums (for example, in milk, see below) by magnetic extraction of the reacted components followed by redispersing in a suitable medium with subsequent measurements of DLS. Therefore, we used these particles for further studies.

Table 1 Precision of the CAP measurements

CAP concentration (ng/ml)	RSD (%)
29	5.3
57	2.4
286	4.3
571	3.9

The analysis of the results indicates that there is no detectable particle aggregation at very high CAP concentration (1 g/l in the sample solution), and the mean conjugate diameter is similar to that of single nanoparticle. The dependence of AHD on concentration in a semi-log scale is close to linear or parabolic with a small non-linearity in the wide concentration range (Fig. 3a). For relatively small concentrations, the dependence of the nanoparticle AHD on analyte concentration can be fit by the empirical formula:

$$d(c) = d_\infty + \frac{d_0 - d_\infty}{1 + k \cdot C^n} \tag{3}$$

where d_0 is the AHD in the absence of CAP; d_∞ is the AHD at a very high CAP concentration, where no aggregation is detected; and k and n are the fitting parameters, which can be calculated from the experimental data. The examples of this formula application are presented in Fig. 3b. The non-linear least square method was applied for calculation of the fitting parameters k and n. This formula and algorithm can be used to plot the calibration curve for various analytes of interest.

Note that the value of AHD in the analyte absence and at a fixed measurement time can serve as a reliable input test for quality control of the used bioconjugates. In particular, the

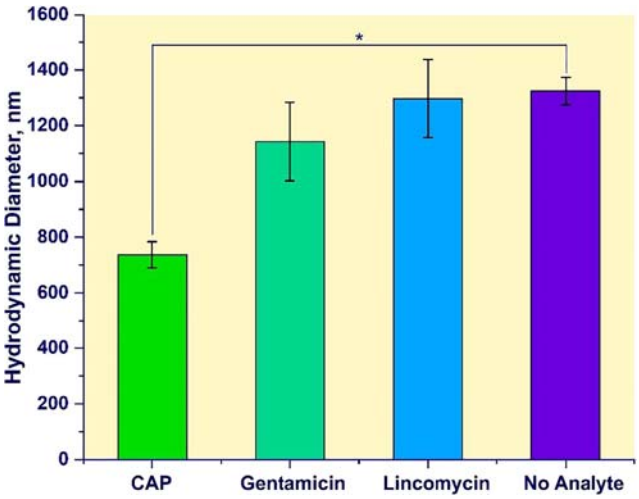

Fig. 4 Results of the nanosensor specificity test. AHD of the reaction suspension after incubation with CAP and two other antibiotics in comparison with a control signal (no analyte added). Asterisks indicate the significance level of the difference ($p < 0.01$) between signal and control

Table 2 Results of the assay recovery study ($n = 5$)

Sample concentration (ng/ml)		Increase in concentration (ng/ml)		Recovery (%)
Unspiked	Spiked	Expected	Found	
53.3	160.0	106.7	103.5	97.0
53.3	293.3	240.0	238.4	99.3
266.7	400.0	133.3	122.3	91.8

values less than 2000 nm after 30-min incubation indicated poor quality of the SPION-based conjugate (for example, its deterioration due to long-term storage) and the need to replace it.

In addition, as can be seen from Fig. 3b and the data in ESM Table S2, the shape and slope of the AHD vs. CAP concentration curve and the sensitivity of CAP determination greatly depend on colloid-chemical properties of the nanoparticles and the resulting bioconjugates. In particular, three different receptor surface densities were studied by changing the concentration of anti-CAP antibody (conjugate A) and CAP-BSA (conjugate B) in the adsorption solution (1.0, 0.33, and 0.11 g/l). Besides, for each density, the measurements of average hydrodynamic diameter at three different volume conjugate A/B ratios (1: 2, 1:1, and 2:1) were made in five repetitions. We found that by varying a number of nanoparticle parameters (size, carboxylic group concentration, amount of surface adsorbed biomolecules, ratio of the components, etc.), we could control the shape and slope of the calibration curve to optimize the assay performance. These results are in good agreement with the proposed mathematical model (Section S.1.3.2 in ESM), given the differences in the value of the parameter q_0 (total number of antibodies per conjugate). In the optimized conditions, the LOD for CAP determination was found to be as low as 4 ng/ml.

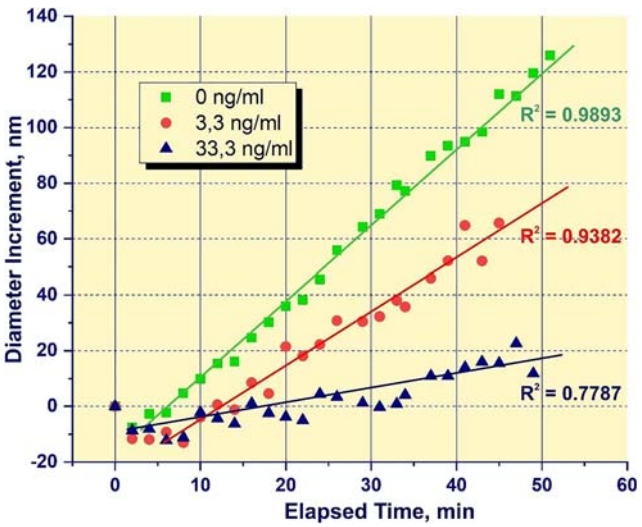

Fig. 5 Time evolution of the AHD increment for different CAP concentrations. DLS results with use of SPION-based conjugates

It is important that the proposed two-stage assay is more resistant to the sample-induced non-specific aggregation than the traditional single-stage competitive format of DLS assay. Indeed, the addition of an analyte reduces the number of vacant antibodies and, accordingly, affects only the biospecific aggregation of the conjugates at the second stage of the analysis. Since the nanosensor detects the change in AHD relative to the particle size at the beginning of the second stage of the assay, the possible non-specific aggregation of nanoparticles or blocking the bioreceptors by the sample components is disregarded and does not affect the result. This also allowed significant expansion of the working concentration range of the sensor, which in our measurements reached the record three orders of magnitude and significantly exceeded the known analogues (see below).

Evaluation of the assay performance

Specificity To test the specificity of the CAP nanosensor, we carried out control experiment to verify the influence of the interfering substances on the nanosensor signal. The solutions of the two commonly used antibiotics – gentamicin and

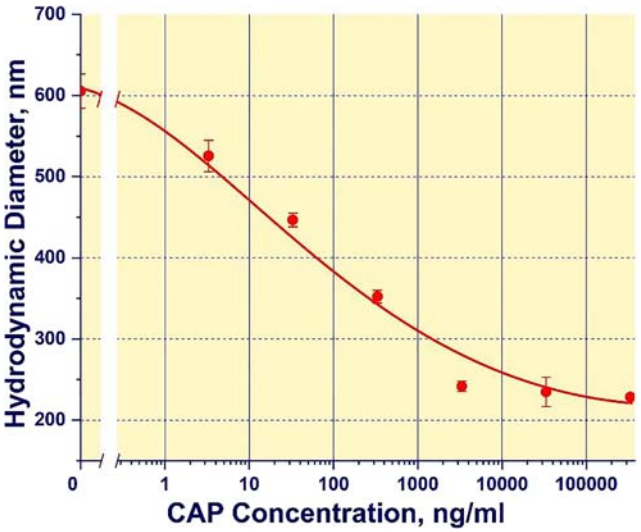

Fig. 6 Dependence of the nanoparticle AHD vs. CAP concentration in milk. SPION-L (lower-carboxylated)-based conjugate A was incubated with CAP-spiked milk samples, then magnetically separated, redispersed in buffer, and incubated with conjugate B, followed by AHD measurements by the ARN-2 DLS analyzer. Error bars correspond to standard deviation

lincomycin – were used as non-specific analytes. For each drug, the same sequence of operations was carried out as for CAP detection using CAP-specific SPION-based conjugates. The results of end point measurements at high (10,000 ng/ml) analyte concentration are presented in Fig. 4. As can be seen, the addition of even large amount of antibiotics other than chloramphenicol does not lead to significant unspecific decrease of AHD. This confirms the good specificity of the nanosensor.

Precision To evaluate the assay precision, five independently prepared CAP samples in the working buffer were obtained for four different CAP concentrations. Each of the samples was analyzed 5 times using a standard DLS technique, and relative standard deviations (RSD) were calculated (Table 1). The RSD for the measurement sets was found to be in the range of 2.4–5.3% with the mean RSD value as small as 4.0 ± 1.2%.

Ruggedness The assay ruggedness against possible variations in sample preparation and instrumentational errors was validated by comparison of the normalized values of AHD for the two series of measurements of independently prepared CAP samples by different DLS instruments (Zetasizer Nano ZS and ARN-2). We found that the mean RSD between the two series was 8.3%.

Recovery Recovery of the assay was determined by analysis of spiked CAP working buffer solutions (see "Methods" section). Three CAP-containing samples with known concentrations were mixed together in equal proportions, and the measured and calculated values were compared using the corresponding calibration curve (Fig. 3b). As can be seen from the typical results (Table 2), the assay recovery was in the range of 92–99% that indicates a good agreement between the measured and calculated values (mean recovery ca. 96%).

Kinetic study of the nanosensor signal evolution

Results of the time dependence measurements of the nanoparticle AHD evolution are shown in Fig. 5. The measurement duration was about 1 h, twice longer than that in the end point detection experiments (see above). An almost linear dependence of AHD vs. time was observed. That is in a good agreement with that predicted by Eq. (2).

Note that the AHD in the time-resolved measurements after 30-min incubation is smaller than that detected in the end point measurements due to lower concentration of antibodies and analyte. The experimental kinetics data shown in Fig. 5 are consistent with the simulation results shown in ESM Fig. S1.

Detection of CAP in real samples

To demonstrate the potential of the proposed method, we analyzed real food samples using CAP-spiked milk as an example. The composition variability, high content of interfering and masking components (fats, proteins, carbohydrates), and heavy turbidity make milk a very difficult object for optical assays. To implement this analysis, we used the advantages of rapid magnetic separation, provided by the use of the conjugates based on magnetic nanoparticles.

According to the developed technique, after sample preparation to separate milk fats (see "Methods" section), a known amount of CAP was added and then incubated with SPION-L conjugate A. After that, the magnetic particles were quickly precipitated using a permanent magnet, redispersed in the working buffer, and incubated with SPION-L conjugate B, and AHD measurements were carried out according to the previously developed protocol (see "Methods" section). The calibration curve constructed in this way is presented in Fig. 6. The LOD calculated using the "3 Sigma" criterion was found to be as low as 2.4 ng/ml with a wide dynamic range of more than 3 orders (5 to 10,000 ng/ml).

We should note that the processing of the non-defatted milk samples may require further adjustment of the assay to account for the lipid-solubility of CAP (which may result in significant loss of CAP during the defatting process) [46].

Comparison with other CAP nanosensors

The comparison of the proposed method with some other reported indirect optical CAP nanosensors is shown in Table 3. It should be noted that several analytical techniques

Table 3 Analytical characteristics of some optical CAP nanosensors

Detection method	Limit of detection (ng/ml)	Concentration range (ng/ml)	Samples	Reference
Quantum dots fluorescence	5	40–500	Serum and milk	[35]
SERS + gold nanoparticles + polymers	100	100–1000	Milk	[36]
LSPR + gold nanoparticles + aptamers	0.01	0.03–3	Milk	[37]
Colorimetry + gold nanoparticles + aptamers	2.5	30–150	Milk	[38]
DLS + magnetic nanoparticles + antibody	2.4	5–10,000	Milk	This work

mentioned in the "Introduction" section provide the limits of CAP detection on the level of about 0.1–1.0 ng/ml. However, these indirect methods are time-consuming and complicated and thus are hardly suitable for express diagnostics (screening). At the same time, having a good sensitivity (up to 2.4 ng/ml) in real samples, a record-wide dynamic range of measured concentrations, and considerable ease of measurement, the proposed nanosensor has obvious advantages over these methods and can be successfully applied to point-of-care diagnostics.

Conclusion

Here, we have demonstrated a novel approach to direct optical biosensing that exploits the DLS-based analysis. The operation concept employs a two-step competition between target molecules in a sample and on the surface of nanoparticles. Developed biosensing method has been confirmed both theoretically by the numerical simulation and experimentally in the end point and kinetic modes. The near-linear dependence of AHD on concentration in semi-log scale has allowed us to reach the record-wide dynamic concentration range of three or more orders of magnitude. The analytical platform is universal and may employ various types of nanoparticle interfaces as demonstrated with gold, latex, and superparamagnetic nanoparticles. Such flexibility has permitted significant expansion of the method functionality, including analyzing of opaque medium such as food products. In particular, the analytical potential of the nanosensor has been confirmed by detection of chloramphenicol antibiotic in milk with high sensitivity (LOD ca. 2.4 ng/ml) within the wide dynamic range (5–10,000 ng/ml). The combination of sensitivity, specificity, and reproducibility of the proposed method makes it a promising tool for express field environment monitoring and point-of-care diagnostic applications.

Funding information This multidisciplinary work was supported by the grant of Russian Science Foundation no. 16-19-00131 (development and characterization of the nanoparticles and their conjugates with bioreceptors) and Ministry of Science and Higher Education of Russian Federation in the framework of the implementation of agreement no. 14.624.21.0045 of September 26, 2017 (unique identifier RFMEFI62417X0045) (dynamic light scattering assay experiments).

Compliance with ethical standards

Conflict of interest All-Russian Research Institute for Optical and Physical Measurements has filed a patent application RU2019140681 on the developed assay technology (L.A.D., R.A., A.M.K., D.E.B., N.M.P. are named as the inventors).

References

1. Wolfbeis OS. Optical technology until the year 2000: an historical overview. In: Optical sensors. Berlin: Springer Berlin Heidelberg; 2004. p. 1–34.
2. Nikitin PI, Beloglazov AA. A multi-purpose sensor based on surface plasmon polariton resonance in a Schottky structure. Sensors Actuators A Phys. 1994;42:547–52. https://doi.org/10.1016/0924-4247(94)80051-0.
3. Gauglitz G, Homola J. Direct optical detection. Anal Bioanal Chem. 2015;407:3881–2. https://doi.org/10.1007/s00216-015-8577-6.
4. Zourob M, Elwary S, Turner A. Principles of bacterial detection: biosensors, recognition receptors and microsystems. New York: Springer New York; 2008.
5. Du B-A, Li Z-P, Liu C-H. One-step homogeneous detection of DNA hybridization with gold nanoparticle probes by using a linear light-scattering technique. Angew Chem Int Ed. 2006;45:8022–5. https://doi.org/10.1002/anie.200603331.
6. Liu X, Dai Q, Austin L, Coutts J, Knowles G, Zou J, et al. A one-step homogeneous immunoassay for cancer biomarker detection using gold nanoparticle probes coupled with dynamic light scattering. J Am Chem Soc. 2008;130:2780–2. https://doi.org/10.1021/ja711298b.
7. Huang X, Xu Z, Mao Y, Ji Y, Xu H, Xiong Y, et al. Gold nanoparticle-based dynamic light scattering immunoassay for ultrasensitive detection of Listeria monocytogenes in lettuces. Biosens Bioelectron. 2015;66:184–90. https://doi.org/10.1016/j.bios.2014.11.016.
8. Dai Q, Liu X, Coutts J, Austin L, Huo Q. A one-step highly sensitive method for DNA detection using dynamic light scattering. J Am Chem Soc. 2008;130:8138–9. https://doi.org/10.1021/ja801947e.
9. Kalluri JR, Arbneshi T, Afrin Khan S, Neely A, Candice P, Varisli B, et al. Use of gold nanoparticles in a simple colorimetric and ultrasensitive dynamic light scattering assay: selective detection of arsenic in groundwater. Angew Chem Int Ed. 2009;48:9668–71. https://doi.org/10.1002/anie.200903958.
10. Borisov SM, Wolfbeis OS. Optical biosensors. Chem Rev. 2008;108:423–61. https://doi.org/10.1021/cr068105t.
11. Nikitin MP, Shipunova VO, Deyev SM, Nikitin PI. Biocomputing based on particle disassembly. Nat Nanotechnol. 2014;9:716–22. https://doi.org/10.1038/nnano.2014.156.
12. Tregubov AA, Nikitin PI, Nikitin MP. Advanced smart nanomaterials with integrated logic-gating and biocomputing: dawn of theranostic nanorobots. Chem Rev. 2018;118:10294–348. https://doi.org/10.1021/acs.chemrev.8b00198.
13. Sokolov IL, Cherkasov VR, Tregubov AA, Buiucli SR, Nikitin MP. Smart materials on the way to theranostic nanorobots: molecular machines and nanomotors, advanced biosensors, and intelligent vehicles for drug delivery. Biochim Biophys Acta Gen Subj. 2017;1861:1530–44. https://doi.org/10.1016/j.bbagen.2017.01.027.
14. Cherkasov VR, Mochalova EN, Babenyshev AV, Vasilyeva AV, Nikitin PI, Nikitin MP. Nanoparticle beacons: supersensitive smart materials with on/off-switchable affinity to biomedical targets. ACS Nano. 2020;14:1792–803. https://doi.org/10.1021/acsnano.9b07569.
15. Jans H, Liu X, Austin L, Maes G, Huo Q. Dynamic light scattering as a powerful tool for gold nanoparticle bioconjugation and biomolecular binding studies. Anal Chem. 2009;81:9425–32. https://doi.org/10.1021/ac901822w.
16. Zheng T, Bott S, Huo Q. Techniques for accurate sizing of gold nanoparticles using dynamic light scattering with particular application to chemical and biological sensing based on aggregate formation. ACS Appl Mater Interfaces. 2016;8:21585–94. https://doi.org/10.1021/acsami.6b06903.

17. Seow N, Tan YN, Yung L-YL. Gold nanoparticle-dynamic light scattering tandem for the rapid and quantitative detection of the let7 microRNA family. Part Part Syst Charact. 2014;31:1260–8. https://doi.org/10.1002/ppsc.201400158.
18. Seow N, Tan YN, Yung L-YL SX. DNA-directed assembly of nanogold dimers: a unique dynamic light scattering sensing probe for transcription factor detection. Sci Rep. 2016;5:18293. https://doi.org/10.1038/srep18293.
19. Li C, Ma J, Fan Q, Tao Y, Li G. Dynamic light scattering (DLS)-based immunoassay for ultra-sensitive detection of tumor marker protein. Chem Commun. 2016;52:7850–3. https://doi.org/10.1039/C6CC02633H.
20. Zheng T, Pierre-Pierre N, Yan X, Huo Q, Almodovar AJO, Valerio F, et al. Gold nanoparticle-enabled blood test for early stage cancer detection and risk assessment. ACS Appl Mater Interfaces. 2015;7:6819–27. https://doi.org/10.1021/acsami.5b00371.
21. Mustafaoglu N, Kiziltepe T, Bilgicer B. Site-specific conjugation of an antibody on a gold nanoparticle surface for one-step diagnosis of prostate specific antigen with dynamic light scattering. Nanoscale. 2017;9:8684–94. https://doi.org/10.1039/C7NR03096G.
22. Huo Q, Litherland SA, Sullivan S, Hallquist H, Decker DA, Rivera-Ramirez I. Developing a nanoparticle test for prostate cancer scoring. J Transl Med. 2012;10:44. https://doi.org/10.1186/1479-5876-10-44.
23. Driskell JD, Jones CA, Tompkins SM, Tripp RA. One-step assay for detecting influenza virus using dynamic light scattering and gold nanoparticles. Analyst. 2011;136:3083. https://doi.org/10.1039/c1an15303j.
24. Zheng T, Finn C, Parrett CJ, Dhume K, Hwang JH, Sidhom D, et al. A rapid blood test to determine the active status and duration of acute viral infection. ACS Infect Dis. 2017;3:866–73. https://doi.org/10.1021/acsinfecdis.7b00137.
25. Lai YH, Koo S, Oh SH, Driskell EA, Driskell JD. Rapid screening of antibody–antigen binding using dynamic light scattering (DLS) and gold nanoparticles. Anal Methods. 2015;7:7249–55. https://doi.org/10.1039/C5AY00674K.
26. Gao D, Sheng Z, Han H. An ultrasensitive method for the detection of gene fragment from transgenics using label-free gold nanoparticle probe and dynamic light scattering. Anal Chim Acta. 2011;696:1–5. https://doi.org/10.1016/j.aca.2011.04.001.
27. Fu C, Ma H, Huang C, Jia N. A simple and dual functional dynamic light scattering (DLS) probe for rapid detection of mercury ions and biothiols. Anal Methods. 2015;7:7455–60. https://doi.org/10.1039/C5AY01880C.
28. Huang X, Liu Y, Yung B, Xiong Y, Chen X. Nanotechnology-enhanced no-wash biosensors for in vitro diagnostics of cancer. ACS Nano. 2017;11:5238–92. https://doi.org/10.1021/acsnano.7b02618.
29. Orlov AV, Nikitin MP, Bragina VA, Znoyko SL, Zaikina MN, Ksenevich TI, et al. A new real-time method for investigation of affinity properties and binding kinetics of magnetic nanoparticles. J Magn Magn Mater. 2015;380:231–5. https://doi.org/10.1016/j.jmmm.2014.10.019.
30. Ivanov AE, Pushkarev AV, Orlov AV, Nikitin MP, Nikitin PI. Interferometric detection of chloramphenicol via its immunochemical recognition at polymer-coated nano-corrugated surfaces. Sensors Actuators B Chem. 2019;282:984–91. https://doi.org/10.1016/j.snb.2018.11.043.
31. Sai N, Chen Y, Liu N, Yu G, Su P, Feng Y, et al. A sensitive immunoassay based on direct hapten coated format and biotin–streptavidin system for the detection of chloramphenicol. Talanta. 2010;82:1113–21. https://doi.org/10.1016/j.talanta.2010.06.018.
32. Brox S, Ritter AP, Küster E, Reemtsma T. A quantitative HPLC–MS/MS method for studying internal concentrations and toxicokinetics of 34 polar analytes in zebrafish (Danio rerio) embryos. Anal Bioanal Chem. 2014;406:4831–40. https://doi.org/10.1007/s00216-014-7929-y.
33. Dams ET, Laverman P, Oyen WJ, Storm G, Scherphof GL, van Der Meer JW, et al. Accelerated blood clearance and altered biodistribution of repeated injections of sterically stabilized liposomes. J Pharmacol Exp Ther. 2000;292:1071–9.
34. Sun M, Ding B, Lin J, Yu J, Sun G. Three-dimensional sensing membrane functionalized quartz crystal microbalance biosensor for chloramphenicol detection in real time. Sensors Actuators B Chem. 2011;160:428–34. https://doi.org/10.1016/j.snb.2011.08.004.
35. Amjadi M, Jalili R, Manzoori JL. A sensitive fluorescent nanosensor for chloramphenicol based on molecularly imprinted polymer-capped CdTe quantum dots. Luminescence. 2016;31:633–9. https://doi.org/10.1002/bio.3003.
36. Xie Y, Zhao M, Hu Q, Cheng Y, Guo Y, Qian H, et al. Selective detection of chloramphenicol in milk based on a molecularly imprinted polymer-surface-enhanced Raman spectroscopic nanosensor. J Raman Spectrosc. 2017;48:204–10. https://doi.org/10.1002/jrs.5034.
37. Javidi M, Housaindokht MR, Verdian A, Razavizadeh BM. Detection of chloramphenicol using a novel apta-sensing platform based on aptamer terminal-lock in milk samples. Anal Chim Acta. 2018;1039:116–23. https://doi.org/10.1016/j.aca.2018.07.041.
38. Wu Y, Liu B, Huang P, Wu F-Y. A novel colorimetric aptasensor for detection of chloramphenicol based on lanthanum ion–assisted gold nanoparticle aggregation and smartphone imaging. Anal Bioanal Chem. 2019. https://doi.org/10.1007/s00216-019-02149-7.
39. Saha B, Evers TH, Prins MWJ. How antibody surface coverage on nanoparticles determines the activity and kinetics of antigen capturing for biosensing. Anal Chem. 2014;86:8158–66. https://doi.org/10.1021/ac501536z.
40. Gambinossi F, Mylon SE, Ferri JK. Aggregation kinetics and colloidal stability of functionalized nanoparticles. Adv Colloid Interf Sci. 2015;222:332–49. https://doi.org/10.1016/j.cis.2014.07.015.
41. Holthoff H, Egelhaaf SU, Borkovec M, Schurtenberger P, Sticher H. Coagulation rate measurements of colloidal particles by simultaneous static and dynamic light scattering. Langmuir. 1996;12:5541–9. https://doi.org/10.1021/la960326e.
42. Shevchenko KG, Cherkasov VR, Nikitina IL, Babenyshev AV, Nikitin MP. Smart multifunctional nanoagents for in situ monitoring of small molecules with a switchable affinity towards biomedical targets. Appl Nanosci. 2018;8:195–203. https://doi.org/10.1007/s13204-018-0659-2.
43. Guteneva NV, Znoyko SL, Orlov AV, Nikitin MP, Nikitin PI. Rapid lateral flow assays based on the quantification of magnetic nanoparticle labels for multiplexed immunodetection of small molecules: application to the determination of drugs of abuse. Microchim Acta. 2019;186:621. https://doi.org/10.1007/s00604-019-3726-9.
44. Shevchenko KG, Cherkasov VR, Tregubov AA, Nikitin PI, Nikitin MP. Surface plasmon resonance as a tool for investigation of non-covalent nanoparticle interactions in heterogeneous self-assembly & disassembly systems. Biosens Bioelectron. 2017;88:3–8. https://doi.org/10.1016/j.bios.2016.09.042.
45. Levin AD, Shmytkova EA. Nonspherical nanoparticles characterization by partially depolarized dynamic light scattering. Proc SPIE. 2015;9526:95260P. https://doi.org/10.1117/12.2184867.
46. National Center for Biotechnology Information (accessed on Mar. 12, 2020) PubChem Database. Chloramphenicol, CID=5959, https://pubchem.ncbi.nlm.nih.gov/compound/Chloramphenicol.